

# Chapter 11

## Active Fibre Mode-locked Lasers in Synchronization for STED Microscopy



Shree Krishnamoorthy, S. Thiruthakathevan and Anil Prabhakar

**Abstract** Mode-locked fibre ring lasers can generate picosecond optical pulse widths with MHz repetition rates. Applications in optical imaging, or in experiments with pump-probe lasers, benefit from being able to synchronize two lasers at high repetition rates, while retaining the narrow optical pulse widths. We investigate the characteristics of an actively mode-locked fibre ring laser, designed as a slave laser and driven by a commercial Ti:Sapphire laser acting as a master. The master-slave synchronization was stabilized for frequency detuning by matching the cavity lengths, and the dependence of the output pulse width of the slave laser was studied as its cavity was detuned. The increase in pulse width was asymmetric about the ring cavity resonance frequency, a phenomenon that we were able to establish as a consequence of an asymmetry in the detuning range of the higher order cavity modes. We observed that the detuning range decreased linearly with the mode number, an observation that was supported by a theoretical perturbative analysis of cavity locking.

### 11.1 Introduction-Nanoscopy and Lasers

Microscopy has seamlessly adopted laser sources to improve imaging. They have been challenging the theoretical boundaries of traditional microscopy to improve the image resolution to nanometers. With continued advancements, microscopic imaging has transitioned to nanoscale imaging, and the field is now aptly being referred to as nanoscopy. To image finer structures, scanning tunneling microscopes (STM) [1] and UV based microscopes have moved to wavelengths below the visible spectrum. However, such techniques are not compatible with live cell imaging as the absorption

---

S. Krishnamoorthy (✉) · A. Prabhakar  
Indian Institute of Technology, Chennai, India  
e-mail: [shree.krishnamoorthy@gmail.com](mailto:shree.krishnamoorthy@gmail.com)

S. Thiruthakathevan  
Valarkathir Creatronics Private Limited, Chennai, India

© Springer Nature Switzerland AG 2019  
P. Ribeiro et al. (eds.), *Optics, Photonics and Laser Technology 2017*,  
Springer Series in Optical Sciences 222,  
[https://doi.org/10.1007/978-3-030-12692-6\\_11](https://doi.org/10.1007/978-3-030-12692-6_11)

and scattering is very high [2]. Consequently, advanced microscopy using superlenses and other artificially created materials [3, 4] are being pursued.

Fluorescent microscopy is widely used, and preferred, as a method to label the proteins of interest. This allows us to study specific phenomena dealing with interactions of molecules in live cells and tissues. However, fluorescent microscopy is limited in spatial resolution by Abbe's limit. Techniques such as structured illumination microscopy rely on the mathematical nature of the imaging instruments and improve the resolution in the post-processing stage [5] e.g. we can use a Moiré pattern to preserve the phase information in the widefield image. Some techniques rely on intensity dependent non-linear interactions like two-photon (2p) and multi-photon [6] absorption within the sample. Similarly, total internal reflection (TIRF) microscopes uses evanescent optical fields to achieve finer resolutions [7]. Near field optics is also used in near-field scanning optical microscopy (NSOM) for nanoscopy. Other techniques, such as photoactivated localization microscopy (PALM) and stochastic optical reconstruction microscopy (STORM), allow a very small fraction of the illuminated molecules to fluoresce, while keeping the a spatially selected illuminated population in dark state using a patterned laser like RESOLFT, GSD and STED [8–10].

### 11.1.1 STED with Pulsed Lasers

STED is a fast, all optical technique for nanoscopy imaging [11], wherein the fluorescent molecules are de-excited using a depletion laser [8, 12]. The depletion photons interact with the excited molecules only at the periphery of the excitation spot, suppressing the fluorescence there. As a result, only the molecules at the center will fluoresce, cause the imaged spot size to reduce. The suppression of fluorescence is intensity dependent and the effective spot size becomes

$$d \approx \left( \frac{\lambda}{2n \sin \alpha} \right) \frac{1}{\sqrt{1 + \frac{I_d}{I_s}}}. \quad (11.1)$$

This is merely Abbe's resolution, further reduced by depletion laser intensity  $I_d$  when compared to the saturation intensity  $I_s$  [13]. The mechanism of STED is explained in Fig. 11.1.

For a typical fluorophore (fluorescein here), there are two absorption regions, the first is the single photon excitation, or just excitation and another is the 2p excitation. The emission region is shown for the fluorophore. The depletion laser is shaped into a donut and superposed on the sample with the excitation 2p laser spot, as shown in the spatial domain in Fig. 11.1. 2p excitation occurs as usual and the fluorescence intensity decreases typically as shown in the temporal panel. However, in the yellow regions with strong overlap between the depletion and the excitation, the fluorescence

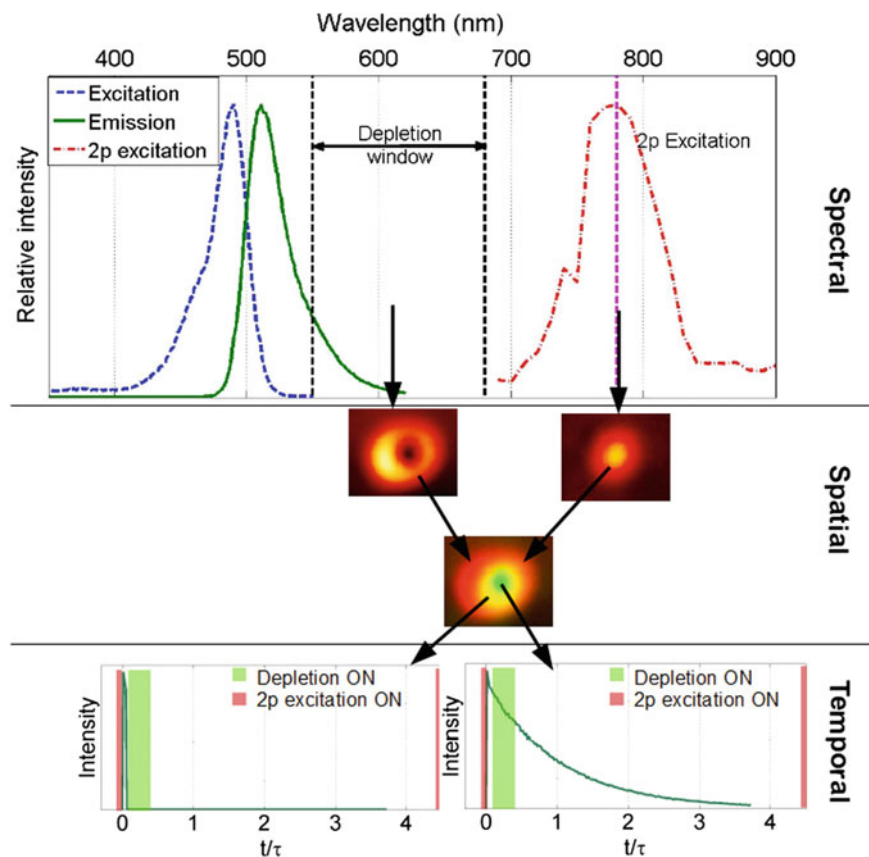


**Fig. 11.1** Summary of 2-photon (2p) STED process. In the spectral domain, we see the excitation and 2p excitation spectra and the emission spectrum. Spatially the donut STED beam of wavelength in the depletion window superposes the 2p excitation spot. Yellow shows significant overlap regions. Temporally the fluorescence trace for one excitation cycle is shown. Red pulses are excitation, green are depletion pulses, and the dark green time trace is the resulting fluorescence. The center of the excitation is unaffected, whereas the peripheral regions experience quenching by the depletion laser

is suppressed and the excited molecules are stimulated emission depleted by the depletion laser as shown to the left of the temporal traces.<sup>1</sup> Although the resolution is enhanced with higher depletion laser intensities, we cannot arbitrarily increase the power of the depletion laser. With increased photon energies on the biological sample, there is an increase in photo-bleaching and thermal damage. One way to minimize these effects is to use pulsed lasers which can deliver high energies for a short duration, typically hundreds of picosecond to nanosecond pulses, reducing the average energy incident on the sample. The pulsed excitation also allows for one to use gated detection, by operating the detector at high gains over short durations. This

<sup>1</sup>The depletion trace in Fig. 11.1 is a simulation using actual fluorescence traces, not actual data.

reduces noise in the images by leaving out the undepleted fluorescent molecules [14]. 2p excitation has been used with CW depletion in STED [15–17]. Here, an IR pulsed laser is used to excite the fluorescent molecules. The small focal volumes in which the fluorophores are excited in a two-photon process, the photo-bleaching is reduced. As an added advantage, light scatters less at longer wavelengths as it propagates in an aqueous medium, thus allowing excitation from deeper within a tissue sample.

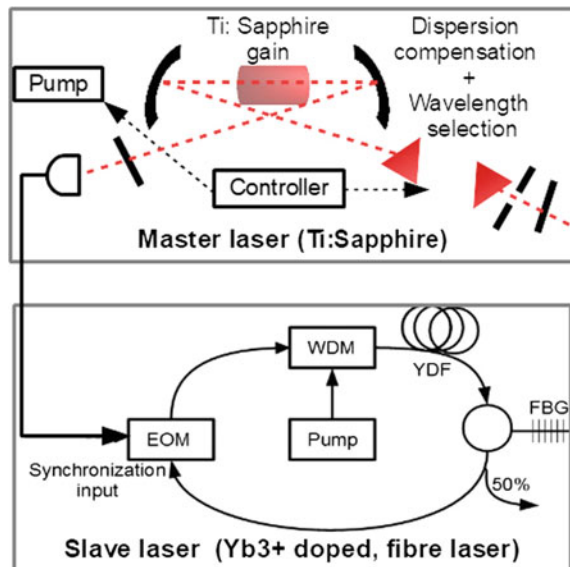
### 11.1.2 Pulsed Fibre Lasers for Synchronization

We focus on the problem of designing and operating two synchronized pulsed lasers to realize a pulsed STED with 2p excitation and pulsed depletion. 2p excitation is typically done using femto-second pulses from commercial Ti:Sapphire passive mode-locked lasers.

The excitation and the depletion lasers need to be synchronized. This is achieved by setting up an interaction between the two laser cavities as shown in Fig. 11.2. The synchronization signal can be in optical or RF domains. Optical synchronization imposes certain demands on the slave lasers, as they will need to produce consistent optical pulses over the operation range of the master. Typical design considerations could be

- pulse to pulse synchronization,
- wavelength restriction,
- pulse widths,

**Fig. 11.2** Schematic of master and slave lasers in synchronization. Synchronization signal is typically around 80 MHz. The master laser is a commercial Ti:Sapphire laser [18] and the slave is a Yb:doped actively mode-locked laser using RF signal derived from master laser optical pulse train [19]



- pulse energies and
- spectral linewidth.

Of all the items, the key factor required in synchronization is the pulse to pulse correspondence between the master and the slave lasers.

There are different implementations of slave lasers in literature. As a depletion laser, an additional pulse stretching module is adopted that converts a part of the master's femto-second laser output into a picosecond laser [17, 20]. The additional module achieves synchronization, but enforces a restriction on the wavelength of the slave laser as the optics is directly coupled to the optical pulses of the master [21]. In other implementations a separate laser is electronically controlled to achieve optical pulses and synchronization [17, 22].

## 11.2 Actively Mode-locked Fibre Lasers

One way to set up optical synchronization, with a Ti:Sapphire laser as a master and a fibre laser as the slave, is to use a part of the optical pulse energy from the master to injection lock the fibre laser. Fraction spectrum amplification (FSA) extracts and amplifies the spectral energy available above  $1\ \mu\text{m}$  from a Rainbow laser [23] and amplifies it using a ytterbium fibre amplifier. In another approach, we could seed the slave laser with sufficient optical energy from the master laser to induce cross phase modulation, as was demonstrated by synchronizing a ytterbium doped fiber laser to a ns pulsed diode laser [24]. Actively mode-locked lasers are capable of high fidelity synchronization using electronic signals. The generation of the electronic signal uses a negligible fraction of the master's optical signal. To obtain repetition rates in the MHz range, actively fibre mode-locked ring lasers are easily constructed with high stability, and easy thermal management. They are self-starting and can be operated at multiple frequencies through harmonic locking. These features makes them attractive for use as pulsed depletion lasers.

### 11.2.1 History of Actively Fibre Mode-locked Lasers

The evolution of all fibre actively mode-locked lasers is shown pictorially in Fig. 11.3. The fibres were available for the infra-red regime at 1000–1500 nm based on silica. The ability to use silica graded index fibres to form laser cavity was first experimentally demonstrated by Nakazawa et al. [25]. To obtain an all fibre mode-locked laser, the field had to wait for two decades for development of fibre coupled linear components, integrated optical devices and fibre coupled laser diodes. Firstly, with the advances in semiconductor technology, an integrated phase modulator was used to make an actively mode-locked laser at  $1\ \mu\text{m}$  which gave 90 ps pulse width [26]. Soliton pulse compression gave 4 ps at  $1.5\ \mu\text{m}$  in an active cavity that also used fibre couplers and Erbium doped gain fibre [27]. In the following decade, the figure of 8

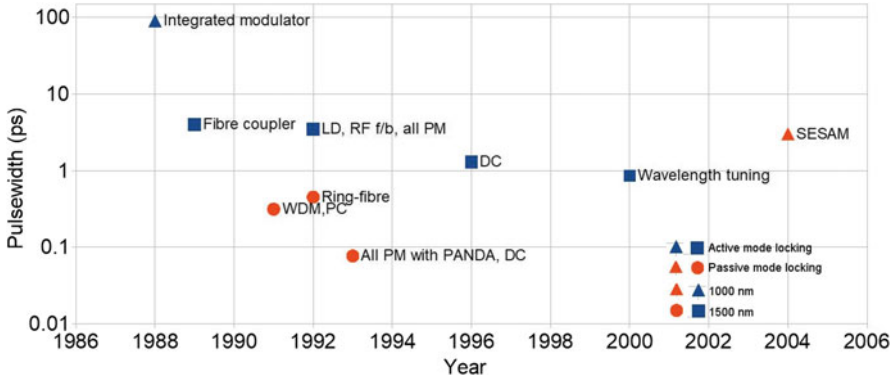


**Fig. 11.3** All fibre actively mode-locked laser’s development over the years. The major changes are shown in the label. The triangles correspond to 1  $\mu\text{m}$  and circles and squares 1.5  $\mu\text{m}$ . Active mode-locking is shown in blue and passive mode-locking in red

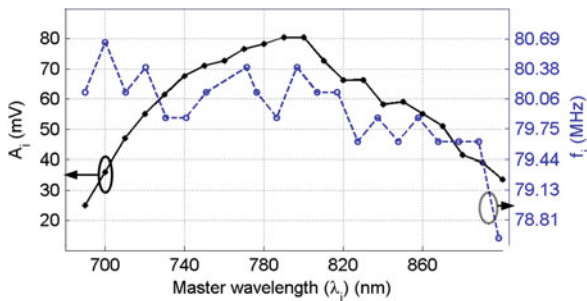
laser (F8L) became popular, and wavelength division multiplexers were available, using this and fibre based polarization control 314 fs passively mode-locked laser was constructed [28]. The ring configuration used by Tamura et al. in the passive mode-locking gave 452 fs pulses and the laser was self starting [29]. In the same year, actively mode-locked lasers were demonstrated with forward, and backward diode laser pumping with fibre pigtailed [30]. RF regenerative feedback control provided the stability in the pulse train. It also was a polarization maintaining cavity. However, the pulse widths in actively mode-locked lasers remained high at 3.5 ps compared to the passive ones. Dispersion compensation using large lengths of positive dispersion fibre compressed the gain stretched pulses. This led to shorter pulse widths in the soliton regime at 77 fs [31]. In actively mode-locked lasers, dispersion compensation was employed [32]. This led to reduction in pulse widths to 1.3 ps. In the next decade, researchers attempted to obtain wavelength tuning in the mode-locked lasers [33], which also set the lower limit on pulse width of mode-locked lasers to about 800 fs. The field of ultrafast lasers saw another entrant with the invention of semiconductor saturable absorber mirrors (SESAM). The rapidly evolving field is described very well by U. Keller in her review paper in 2010 [34]. Both Kerr-lens mode-locking and SESAMs have led to ultrafast lasers in passive mode-locking systems. An early adoption of SESAM based passive mode-locking was demonstrated at 1  $\mu\text{m}$  by [35]. With the advances in as listed in the previous paragraph, a typical actively mode-locked laser configuration can now be depicted as shown in Fig. 11.2. Another method of all fibre active mode-locking could be considered to be the pulses generated by cross-phase modulation (XPM). Pulses generated by this method rely on the nonlinear interaction between injected source pulse and the pulses in the nonlinear cavity through XPM process [36].

### 11.2.2 Active Fibre Mode-locked Laser as Slave

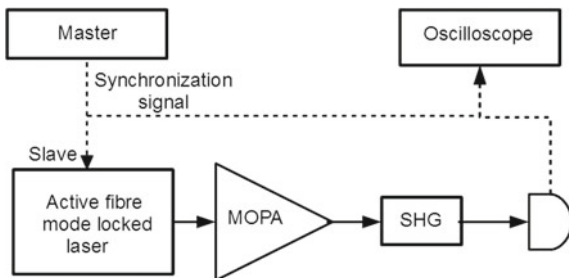
Pulsed electrical signals derived from the Ti:Sapphire were used to injection lock a fibre ring laser (FRL), shown schematically in Fig. 11.2. The FRL was designed to have a cavity resonance close to the repetition rate of the Ti:Sapphire, allowing the FRL to also achieve mode-locking. The slave laser operates at 1064 nm and uses an Yb<sup>3+</sup> doped fiber with an electro-optic modulator (EOM) that acts as the mode-locker [37, 38]. Typically, the Ti:Sapphire wavelength ( $\lambda_i$ ) is tuned between wavelength ranges 690–1020 nm to obtain the best two-photon excitation of the fluorophore. The electrical synchronization signal derived from the master optical signal varies in amplitude  $A_i$  and frequency  $f_i$  as shown in Fig. 11.4. As  $\lambda_i$  is changed,  $f_i$  also changes between 78.8 and 80.7 MHz, with  $A_i$  reaching a maximum for  $\lambda_i \sim 800$  nm [37].

We observed that the pulse width of the slave FRL varied over the wavelength range of the master, due to a changing repetition rate of the master laser pulses. This could result in a loss of mode-lock in the FRL. We also observed that the pulse width at the output of the slave FRL varied as the wavelength of the master laser was tuned. To look at the pulse width variation, we took advantage of the sensitivity of nonlinear processes to the peak pulse intensity, and documented the average power at the output of a second harmonic generation (SHG) stage as shown in Fig. 11.5 [37]. The output of the FRL was amplified by 21 dB using two amplifier stages consisting of a Yb: fiber amplifier followed by a master oscillator power amplifier (MOPA). The amplified output was then fed to a SHG stage to produce pulses at 532 nm. The

**Fig. 11.4** Synchronization signal voltage ( $A_i$ ) and frequency ( $f_i$ ) with changing operating wavelength ( $\lambda_i$ ) of the master laser [37, 39].



**Fig. 11.5** Schematic to monitor the output from a slave laser. Second harmonic generation is inherently sensitive to the intensity of the pulses [39]



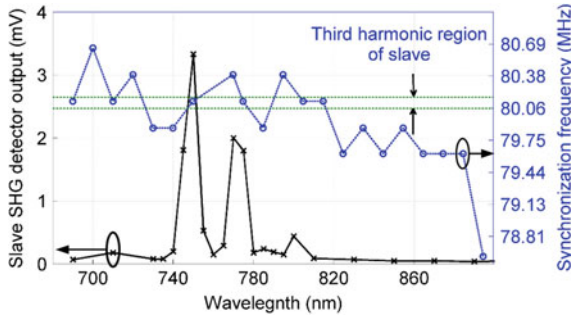


**Fig. 11.6** Dependence of Ti:S pulse repetition rate and its effect on SHG power. A peak in SHG occurs when the Ti:S repetition frequency,  $f_i$ , matches the third harmonic of the slave laser [37, 39]

recorded peak pulse amplitude at the detector  $A_{SHG}$  corresponding to the SHG optical power  $P_{SHG}$  for different master laser wavelengths is shown in Fig. 11.6. As expected,  $P_{SHG}$  depends on the peak power of the input pulse. Consequently, for a fixed average power in the 1064 nm pulse train,  $P_{SHG}$  will depend nonlinearly on the input pulse width. Hence, the SHG process amplifies the effect of high intensity in the amplified 1064 nm pulses. We observe, in Fig. 11.6, that  $P_{SHG}$  peaks at 750 nm, 770 nm and 805 nm. Near these peaks, the repetition rate,  $f_i \sim 80.07$  MHz, corresponds to the third harmonic frequency ( $f_{3rd_s}$ ) of the slave fiber MLL as indicated by the green lines in the plot.

The peak pulse power and pulse width are not constant in the pulse train produced by the slave laser, as seen in Fig. 11.7. In fact, every third pulse produced by the slave laser has a larger amplitude than the others. A slightly detuned input frequency

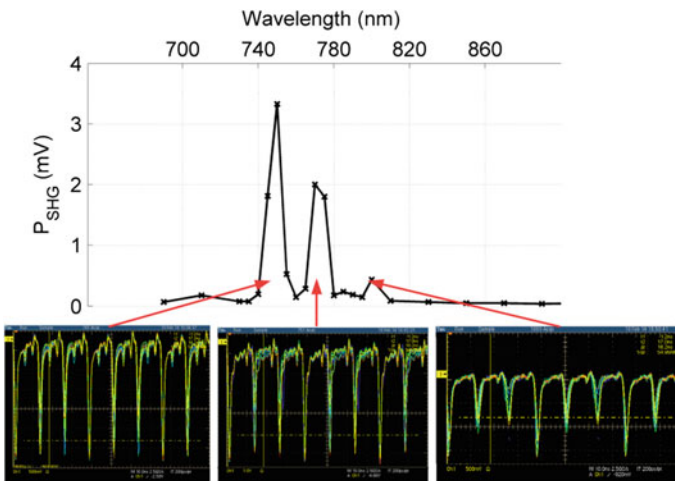


**Fig. 11.7** Slave laser pulse traces for the different operating wavelengths. Every third pulse being intense indicates the dominance of fundamental [37, 39]



$f_i$  in the synchronization signal from the master laser causes a modulation in the slave fiber laser. This can be understood on the basis of effects detuning in a fibre mode-locked laser.

### 11.3 Detuning of Fibre Mode-locked Lasers

Mode-locked lasers produce Fourier limited pulses at resonance [40–42]. The pulse width can be further reduced and soliton regimes are achieved in fibre lasers with addition of nonlinearity [43–45]. However, upon detuning from the mode-locking frequency, the behavior of the laser departs from the ideal mode-locked state.

#### 11.3.1 Deterioration of Mode-locking with Detuning

Deterioration of mode-locking is best understood in actively mode-locked lasers, as they can be driven with sinusoid generators. In a typical case of use as slave laser, the repetition rate of the synchronization signal  $f_i$  varies over a range of  $\sim 100$  kHz. The slave fiber laser is expected to operate over this range. The effect of changing repetition rate  $f_i$  is studied by changing the frequency of the input signal to the EOM of the fiber laser using a signal generator [37].

Behavior of a typical actively mode-locked laser upon detuning is shown in Fig. 11.8. Fourier limited pulses are observed at the mode-locking frequency, this yields the shortest pulses and highest energies. Detuning on both sides of the mode-locking frequency causes increase in pulse width and a decrease in pulse energy, this is due to systematic lock-loss in the modes of the laser. Upon further detuning, locking in any mode is completely lost, and the laser is just modulated. In this case, the pulse width is the same as the modulation signal coming from synchronization pulses. In summary, the ring cavity modes that combine to form the optical pulses fall into a mode-locked regime, in a narrow frequency range about the cavity resonance,

**Fig. 11.8** Average power and pulse width over the expected operating range of slave laser [37, 39]

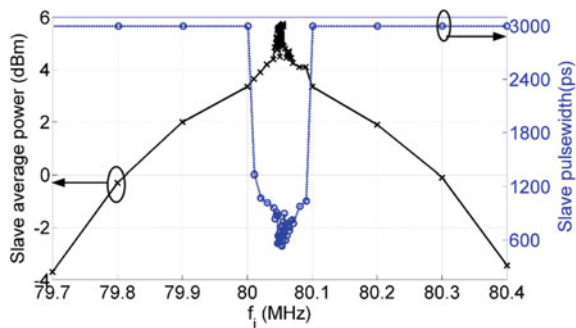
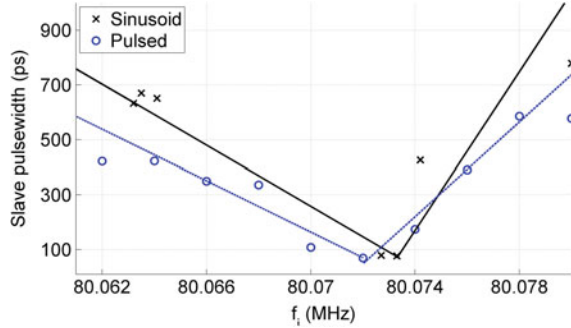


**Fig. 11.9** Closer look at effect of detuning on pulse width around  $f_{3rd_s}$  [37, 39]



and a modulated regime where broader optical pulses are observed. It has to be noted that the operating regimes of the fiber laser depend on the repetition rate of the master laser’s synchronization signal. For wavelength tunable cavities which are optimized for maximizing signal power, the repetition rate varies over a wide range, which will affect the performance of the slave laser. A wavelength independent synchronization mechanism that relies on the active mode-locking phenomenon offers us the ability to synchronize two pulsed lasers over a wide range of repetition rates. One way to ensure that locking is possible is to use optical delays in the laser cavity [46]. If the cavity length of the fiber cavity is maintained, then the operating frequency of the master laser needs to be within the detuning range of all the slave cavity. The narrowest pulses have a pulse width ( $\tau$ ) corresponding to the perfectly mode-locked laser at the mode-locking frequency  $f_0$ . For frequency bandwidth  $f_B$  [42],  $\tau$  is given by

$$\tau = \tau_0 \cdot \left( \frac{1}{f_0 f_B} \right)^{1/2} . \tag{11.2}$$

Here, the  $\tau_0$  is determined by the gain and modulation depth. The pulse width deterioration due to detuning can be seen for both pulsed and sinusoidal signals in Fig. 11.9. The increase in pulse width is not symmetrical about  $f_0$  for either sinusoidal or pulsed RF inputs. Slopes for the pulse width change for frequencies  $f_i > f_0$  is found to be twice as that for  $f_i < f_0$ . In another demonstration of self-mode locking laser by Thiruthakkathevan [47], two different measurement schemes were used. One measured the pulse width of the pulses generated by using an optical detector followed by an amplifier (LNTIA) followed by a comparator that generated square pulses corresponding to the pulse width of the pulses. This was followed by a low pass filter with a buffer (MVE), that extracted the mean pulse width over many pulses. This scheme of pulse width measurement is incorporated as a feedback component in Fig. 11.10. Another method was to measure the total power content of the higher harmonics. To achieve this, the lower frequency components that include the primary mode and the second harmonic are filtered out before obtaining the average powers. The resultant power measured is due to only the higher modes which is a more reliable indicators

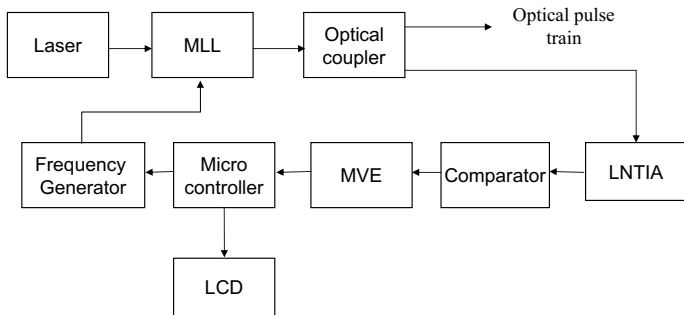


Fig. 11.10 Block diagram of the SMLL, for the pulse width measurement method [47]

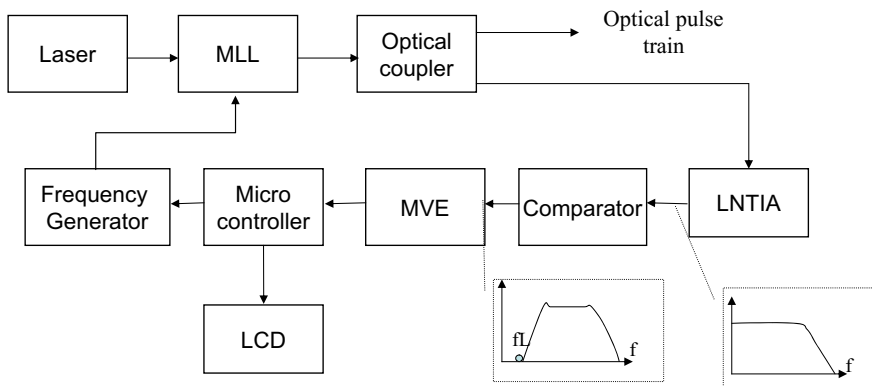
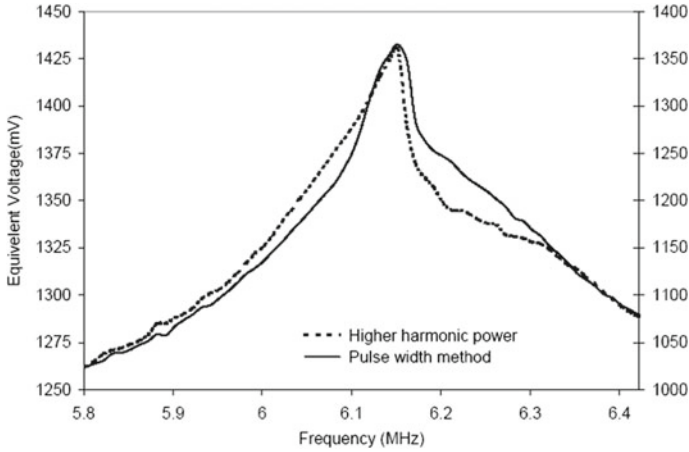


Fig. 11.11 Schematic circuit used to lock the laser cavity by measuring the RF power in the higher harmonics

of mode-locking. This scheme is shown in Fig. 11.11. The asymmetry in pulse width is also found for this  $\text{Er}^{3+}$  doped mode-locked laser in both methods, as shown in Fig. 11.12. Since, the asymmetry is present for both Yb doped, with FBG limited spectrum, and Er doped lasers, we can assume that it is not an intrinsic property of the rare-earth doped fibre. Rather, we believe that the asymmetry is intrinsic to the method of active mode-locking, and is analogous to similar effects reported in electrical circuits [48]. For harmonic locking at  $nf_0$ , the fundamental mode dominates and, and manifests itself as an amplitude modulation on the optical pulse train as shown in Fig. 11.7 (Table 11.1).

### 11.3.2 Loss of locking in Fourier Space

From Fourier theory, we know that while the lowest frequency components in a spectrum contribute to power and slow varying attributes of the pulses, the pulse



**Fig. 11.12** Asymmetric detuning is also present in  $\text{Er}^{3+}$  doped actively mode-locked ring laser [47]

width is determined by the higher frequency components. For a Fourier limited pulse, the frequency components of the pulse will be at multiples of the repetition rate of the pulse, i.e for an input frequency of  $f_i$ , the electrical field amplitude can be described as

$$p(t) = \sum_n A_n \exp(j2\pi n f_i t), \tag{11.3}$$

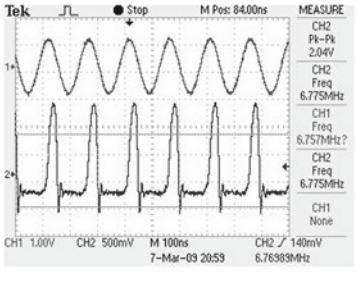
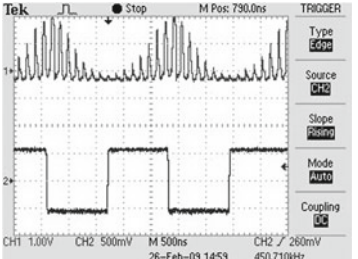
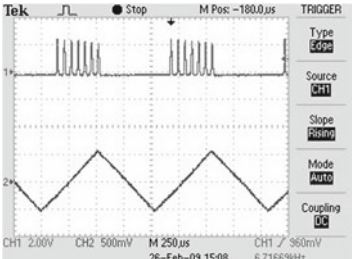
where for the  $n^{\text{th}}$  harmonic  $A_n$  is the complex amplitude at frequency  $n f_i$ . Thus, the frequency location  $\tilde{f}_n$  of each harmonic  $n$  would show if the pulse is mode-locked or not. For a harmonic mode  $n$ , if the observed frequency location  $\tilde{f}_n$  is same as the expected harmonic frequency of  $n f_i$ , then we can say that the harmonic mode is locked to the input synchronization signal at the frequency  $f_i$ . If the observed frequency  $\tilde{f}_n$  and the expected frequency  $n f_i$  do not match, i.e,

$$\Delta f_n \triangleq \tilde{f}_n - n f_i \tag{11.4}$$

is nonzero, then the mode is not locked. To quantify this, we must look at the electrical spectrum of the pulses and capture the behavior of the harmonics that are first to get unlocked with detuning.

The experimental scheme to observe the Fourier mode is as given in Fig. 11.13 [39]. In this scheme, the location of the peak frequency  $\tilde{f}_n$  and the corresponding amplitude  $A_n$  are recorded for each harmonic (or mode number)  $n$  for the input synchronization signal frequency  $f_i$ . One can observe that at the resonant frequency  $f_0 = 26.69$  MHz the power in all the modes is highest as shown in Fig. 11.14. As the input frequency  $f_i$  is detuned from the resonant frequency, the power in all the modes declines.

**Table 11.1** SMLL output for different RF synchronization inputs

Driving signal type	SMLL output and RF signal	RF in Fourier
Sinusoidal		$\left(\frac{\pi}{j}\right) \delta(f - f_0) - \delta(f + f_0)$
Square		$\sum_{k=-\infty}^{\infty} \left( -\frac{2j}{\pi(2k+1)} \delta(f - (2k+1)f_0) \right)$
Triangular		$\sum_{k=-\infty}^{\infty} \left( -\frac{2}{(\pi(2k+1))^2} \delta(f - (2k+1)f_0) \right)$

The oscilloscope traces show both the SMLL pulses and the input RF traces. The corresponding Fourier representation of the RF input is also shown [47]

For each input frequency  $f_i$ , the peak frequency location, for each mode  $n$ , is at  $\tilde{f}_n$ . The deviation  $\Delta f_n$ , from the expected frequency location  $nf_i$ , was defined in (11.4). Figure 11.15 is obtained by plotting  $\Delta f_n$  for the different harmonics  $n$ , as the input frequency  $f_i$  is detuned around the resonance  $f_0$ . When  $f_i = f_0$ , all modes follow the expected frequency and  $|\Delta f_n| = 0$  for all  $n$ . The mode-lock persists for a range of input frequencies around the resonance, in a manner typical of injection locked oscillators [48–51]. It has been shown that mode-locked lasers are also injection locked by the action of the modulation a nonlinear mode-locker [40, 41, 52]. The injection locked laser has all the modes in phase when locked at  $f_0$  and  $|\Delta f_n| = 0$  for all the modes  $n$ .

**Fig. 11.13** Schematic for finding the electrical amplitude spectrum for the modes of the pulses [39]

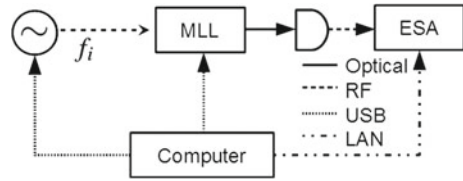


**Fig. 11.14** Amplitude  $A_n$  for each mode  $n$  of the pulse as the input frequency  $f_i$  is varied around the resonance  $f_0 = 26.69$  MHz [39]

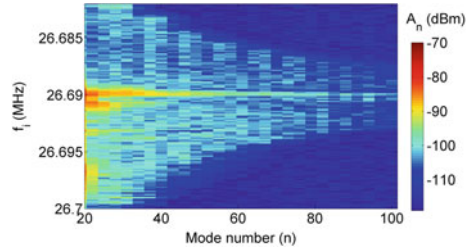
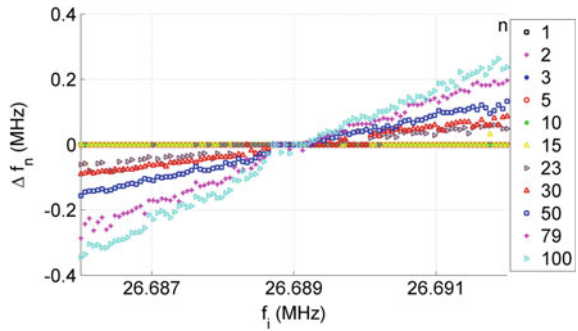
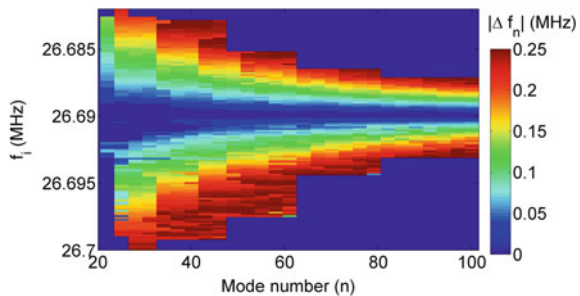


**Fig. 11.15** Deviation  $\Delta f_n$  of each mode  $n$  around the resonance. Lower modes do not deviate in the narrow detuning range and the higher modes deviate faster than the lower modes [39]



However, when detuned, the higher modes are out of the injection range and are the first to lose lock. In these modes the deviation  $|\Delta f_n| > 0$ . The deviations in higher modes build up at a faster rate than for lower modes. This implies that the injection locking is dependent on  $n$  [39]. This can be observed in Fig. 11.16. Both upper and lower limits decrease as mode number increases, indicating that the injection range

**Fig. 11.16** Frequency deviation  $|\Delta f_n|$  for each mode  $n$  of the pulse as the input frequency  $f_i$  is varied around the resonance  $f_0 = 26.69$  MHz [39]



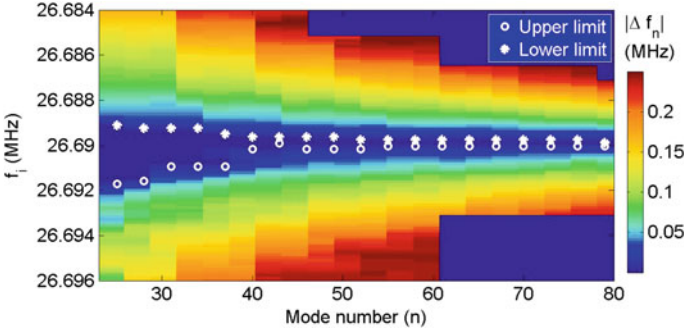


**Fig. 11.17** Upper ( $f_{(U,n)}$ ) and lower ( $f_{(L,n)}$ ) limits of the injection region [39, 53]

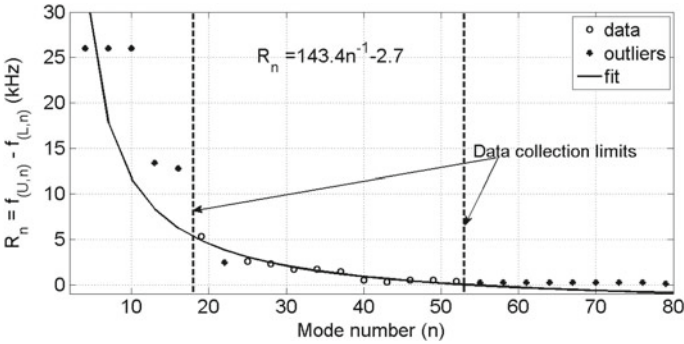


**Fig. 11.18** Injection range  $R_n$  for each mode  $n$ , showing the dependency on the mode number. Modified from [53]

narrows for higher modes. However, the slope of decrease for upper limit is larger by about three times when compared to the lower limit. The region where the deviation in the frequency is nearly zero is the region with mode-locking for any given mode, this is recognized as the the injection range  $R_n$  of the mode  $n$  [40, 41, 49, 50]. The range  $R_n$  is bound by an upper frequency ( $f_{(U,n)}$ ) and a lower frequency ( $f_{(L,n)}$ ).  $R_n$  is defined as

$$R_n \triangleq f_{(U,n)} - f_{(L,n)}. \tag{11.5}$$

As expected, upon further detuning away from  $R_n$ , the higher modes start to show non-zero deviation and lose mode-locking. The injection range  $R_n$  for each mode  $n$  is as shown in Fig. 11.18, and is found to decrease with increasing mode number. The reduction in the injection range is proportional to the mode number as  $n^{-1}$  as found by the fit to the ranges. For modes  $>45$ , our observations of injection range were limited to  $\sim 28$  kHz, by our measuring apparatus (Fig. 11.17).

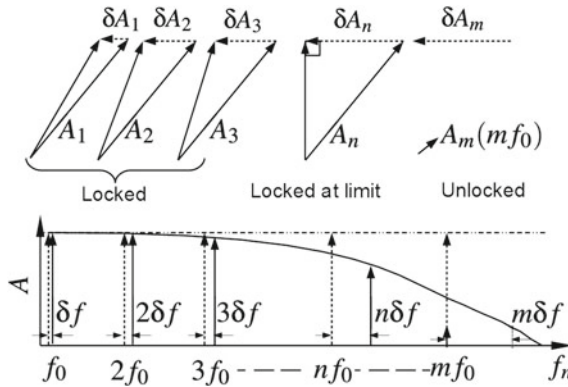


**Fig. 11.19** Effect on cavity mode amplitudes with detuning  $\delta f$ . In the mode amplitude spectra, the mode envelope deviates to the solid line envelope from ideal mode-locked envelope shown in dotted-dashed line. The mode locations in frequency follow the Fourier frequencies of  $(f_n = nf_0 + n\delta f)$ , until mode  $n$ , that is still in the locking limit, the further modes  $(m > n)$  are unlocked and oscillate at  $mf_0$ . The locking limit is where the injection signal is quadrature to the signal in the cavity as shown in the above schematic [39]

### 11.3.3 Unlocking of Laser Modes

The detuning mechanism for a mode-locked laser is shown in Fig. 11.19. For a perfectly mode-locked laser, the modes are at  $f_n = nf_0$ , as shown as dotted delta functions. Upon detuning by  $\delta f$ , the modes occur at  $f_n = nf_0 + n\delta f$ , interpreted as a frequency deviation  $n\delta f$  from the locked state of each mode. The detuned state is shown with solid delta functions in frequency spectrum. Once the frequency deviation  $n\delta f$  is outside the locking range  $R_n$  for the mode, the mode is no longer locked. This is shown for mode  $m$  which is at a higher frequency than the modes  $n$  that are within the locking range. This mode acts as free running oscillator, and the frequency of oscillation is same as at resonance, i.e.  $mf_0$ . However, the phase of the oscillation is no longer related to the rest of the modes [48, 49] and these modes are said to be unlocked.

In the unperturbed, mode-locked state, the amplitudes  $A_n$  for all modes are equal. This makes the spectral envelope of the frequency spectrum uniform, as shown by the dotted horizontal line in Fig. 11.19. The mode amplitudes follow the mode-locking equation for the  $n$ th mode given by Haus as [40]

$$\left\{ 1 + jb + j \frac{nf_i}{f_L} (\sigma + g) - g \left[ 1 - \left( \frac{nf_i}{f_L} \right)^2 \right] \right\} A_n = M (A_{n-1} - 2A_n + A_{n+1}), \tag{11.6}$$



where, quality factor is  $Q$ , and laser linewidth  $f_L$ . The laser gain is  $g$ , the empty-cavity resonance is  $f_C$  and detuning parameter is given by  $\sigma = \frac{2Qf_L}{f_s} \left( \frac{f_i - f_C}{f_i} \right)$ . Any detuning  $\delta f_s$  to the central oscillating frequency  $f_s$  is accounted for by  $b = \frac{2Q}{f_s} \delta f_s$ . When mode-locked  $b = 0$  and  $(\sigma + g) = 0$ . The terms of the right constitute the injection signal due to the action of the modulator with strength  $M$ .

Upon detuning, the spectral envelope deviates from the mode-locked envelope as shown by the solid curve in the frequency spectrum.  $\delta A_n$  for each mode is the change in strength of injection for the mode. It has been shown that the ratios of injection signal to the mode amplitude does not change with the detuning [53]. A portion of the amplitude is required to compensate the phase deviation that builds up with detuning. When the mode frequency  $f_n$  is within the locking range  $R_n$  for the mode, the deviation is the difference phasor between the mode amplitude  $A_n$  at resonance, and the resulting mode amplitude  $A_n + \delta A_n$  after perturbation [48]. The phasors for different modes with respect to the amplitude deviation  $\delta A_n$  are shown at the top of the respective mode at  $nf_0$  in the frequency spectrum. The frequency  $f_n$ , in mode is at the edge of the injection range at either  $f_{(U,n)}$  or  $f_{(L,n)}$ . A condition where the deviation and the resulting amplitude are at quadrature to each other is shown for the mode  $n$  in Fig. 11.19. Using perturbation analysis on (11.6), Krishnamoorthy et al. [53] have shown that  $R_n$  is given by

$$R_n = \left[ \frac{f_s f_0}{Q f_C} \left( \frac{1}{n} \frac{A_{i1}}{A_{o1}} \right) \right], \quad (11.7)$$

where,  $\frac{A_{i1}}{A_{o1}}$  is the ratio of the mode amplitude to the injection signal for the first mode as determined by laser parameters. Which can be further simplified as

$$R_n = R_1 \left( \frac{1}{n} \right). \quad (11.8)$$

where,  $R_1 = \frac{f_s f_0}{Q f_C} \left( \frac{A_{i1}}{A_{o1}} \right)$  is the range for the fundamental mode  $n = 1$ . This equation clearly shows that there is an  $n^{-1}$  dependence on injection range.

A mode  $m$  greater than  $n$  is unlocked, the phasor  $A_m + \delta A_m$  makes an angle greater than  $90^\circ$  with the deviation  $\delta A_m$ . The large phase required to maintain the angle between the injection and the resultant mode amplitude cannot be provided by the laser, thus the mode is not locked and acts as a free running oscillator. The resulting frequency of the unlocked mode is  $mf_0$  and not  $mf_0 + m\delta f$  as would be expected for a locked mode. This is shown by the small delta function at  $mf_0$  in the frequency spectrum in Fig. 11.19. To obtain the narrowest pulses from the slave laser, the repetition rate of the synchronizing master laser needs to be at a harmonic of the locking frequency of the slave laser, with the available detuning range decreasing as  $n$  as we attempt to lock  $n$  cavity modes together.

## 11.4 Conclusion

Fibre lasers are already the focus for adoption for nonlinear microscopy [54]. Other than 2p STED [15, 17], many techniques in time resolved spectroscopy use optical pump and probe methods that involve multiple lasers working in tandem, e.g. in time resolved CARS [55]. Both microscopy with STED and spectroscopy like time resolved coherent anti-Stokes Raman scattering (CARS), require two pulsed lasers working in synchronization to obtain the desired results. This review shows that active fibre mode-locked lasers are an excellent candidate for synchronization with another master laser in the configuration shown in Fig. 11.2. In this review, the authors have focused on using a Ti:Sapphire laser as a master laser, while driving a ytterbium doped fibre (YDF) ring laser in a master-slave configuration using EOM as the mode-locking element.

Actively mode-locked laser is driven using the electrical signal generated from the master laser, which ensures pulse to pulse synchronization. Wavelength selectivity is easily achieved using FBGs in the cavity that restrict the lasing wavelength and linewidth. There are many techniques, like using PZT, that can be employed to tune the wavelength of operation [33]. Other wavelength conversion schemes like second harmonic generation (SHG) or parametric conversion schemes can be used to achieve even wider wavelength options. The pulse energy is increased using fibre amplifiers and master oscillator optical amplifiers (MOPA) as shown in Fig. 11.5. The fibre mode-locked laser can be tuned in active configuration to a large frequency range of  $\sim 500$  kHz, while providing pulse widths in the order of few ps to few ns. At resonant frequencies, they provide the sharpest pulses, that can be further compressed using positive index fibre and other techniques as discussed previously. To obtain uniform pulse trains, methods like regenerative feedback, and higher harmonic power optimization are required to provide the necessary stabilization [33, 47].

For the FRLs to act as slave lasers effectively, it is required that they be operable away from their locking frequencies. This requires a renewed understanding of the detuning mechanism in the lasers. The increase in the pulse width and the decrease in power away from the locking frequencies is discussed here. There is an inherent asymmetry in all FRLs with detuning. The asymmetry in pulse width is shown for Yb:doped FRLs and Er:doped FRLs in Figs. 11.9 and 11.12. The power in the higher modes also decrease asymmetrically as shown with higher harmonic power method. The understanding of the mechanism of the unlocking of lasers is understood by looking at the constituent modes  $n$ . The tolerance to detuning depends on the injection locking range of each mode, which decreases with mode number  $n$  as discussed using experiments and analytically. Further understanding of workings of FRLs is needed to build adaptable fibre lasers for use in biology. While, the lasers find the inroads to biology, the time for bio-inspired lasers has also come [56].

**Acknowledgements** S. Krishnamoorthy thanks Prof. Satyajit Mayor from NCBS-TIFR for guidance and support, the BioEngineering Research Initiative at NCBS for supporting her research and providing the opportunity to be associated with the project. The authors thank Jayavel D., Yusuf Panbharwala and Sathish for help with construction of the lasers. The authors thank Central Imag-

ing and Flow Cytometry Facility (CIFF) at NCBS-TIFR, Bangalore and the photonics@IITM group and Jitu-lab for facilities. Jayant lab and Rama Reddy for support with fluorescence experiments. The authors wish to thank the anonymous reviewers for their valuable suggestions.

## References

1. G. Binnig, H. Rohrer, C. Gerber, E. Weibel, Surface studies by scanning tunneling microscopy. *Phys. Rev. Lett.* **49**, 57–61 (1982)
2. S.L. Jacques, Optical properties of biological tissues: a review. *Phys. Med. Biol.* **58**, R37 (2013)
3. X. Zhang, Z. Liu, Superlenses to overcome the diffraction limit. *Nat. Mater.* **7**, 435 (2008)
4. J.B. Pendry, Negative refraction makes a perfect lens. *Phys. Rev. Lett.* **85**, 3966–3969 (2000)
5. M.G.L. Gustafsson, Surpassing the lateral resolution limit by a factor of two using structured illumination microscopy. *J. Microsc.* **198**, 82–87 (2000)
6. W. Denk, J. Strickler, W. Webb, Two-photon laser scanning fluorescence microscopy. *Science* **248**, 73–76 (1990)
7. D. Axelrod, Cell-substrate contacts illuminated by total internal reflection fluorescence. *J. Cell Biol.* **89**, 141–145 (1981)
8. S.W. Hell, Nobel lecture: nanoscopy with freely propagating light. *Rev. Mod. Phys.* **87**, 1169 (2015)
9. E. Betzig, Single molecules, cells, and super-resolution optics (nobel lecture). *Angew. Chem. Int. Ed.* **54**, 8034–8053 (2015)
10. W.E. Moerner, Single-molecule spectroscopy, imaging, and photocontrol: Foundations for super-resolution microscopy (nobel lecture). *Angew. Chem. Int. Ed.* **54**, 8067–8093 (2015)
11. K. Nienhaus, G.U. Nienhaus, Where do we stand with super-resolution optical microscopy? *J. Mol. Bio.* **428**, 308–322 (2016). Study of biomolecules and biological systems: Proteins
12. S.W. Hell, J. Wichmann, Breaking the diffraction resolution limit by stimulated emission: stimulated-emission-depletion fluorescence microscopy. *Opt. Lett.* **19**, 780–782 (1994)
13. S.W. Hell, Far-field optical nanoscopy. *Science* **316**, 1153–1158 (2007)
14. G. Vicidomini, A. Schönle, H. Ta, K.Y. Han, G. Moneron, C. Eggeling, S.W. Hell, STED nanoscopy with time-gated detection: theoretical and experimental aspects. *PLOS ONE* **8**, 1–12 (2013)
15. J.N. Farahani, M.J. Schibler, L.A. Bentolila, A. Mendez-Vilas, J. Diaz, Stimulated emission depletion (STED) microscopy: from theory to practice. *Microsc. Sci. Technol. Appl. Educ.* **2**, 1539 (2010)
16. T.A. Klar, S. Jakobs, M. Dyba, A. Egner, S.W. Hell, Fluorescence microscopy with diffraction resolution barrier broken by stimulated emission. *Proc. Natl. Acad. Sci.* **97**, 8206–8210 (2000)
17. K.T. Takasaki, J.B. Ding, B.L. Sabatini, Live-cell superresolution imaging by pulsed STED two-photon excitation microscopy. *Biophys. J.* **104**, 770–777 (2013)
18. M.T. Asaki, C.P. Huang, D. Garvey, J. Zhou, H.C. Kapteyn, M.M. Murnane, Generation of 11-fs pulses from a self-mode-locked Ti:sapphire laser. *Opt. Lett.* **18**, 977–979 (1993)
19. A. Prabhakar, S. Mayor, S. Krishnamoorthy, Mode locked laser for generating a wavelength stabilized depletion pulse and method thereof (2014)
20. Y. Wu, X. Wu, L. Toro, E. Stefani, Resonant-scanning dual-color STED microscopy with ultrafast photon counting: a concise guide. *Methods* **88**, 48–56 (2015)
21. M.A. Lauterbach, M. Guillon, A. Soltani, V. Emiliani, STED microscope with spiral phase contrast. *Sci. Rep.* **3**, 2050 (2013)
22. A. Honigmann, S. Sadeghi, J. Keller, S.W. Hell, C. Eggeling, R. Vink, A lipid bound actin meshwork organizes liquid phase separation in model membranes. *eLife* **3**, e01671 (2014)
23. W. Li, Q. Hao, Y. Li, M. Yan, H. Zhou, H. Zeng, Ultrafast laser pulse synchronization, in *Coherence and Ultrashort Pulse Laser Emission* ed. by F.J. Duarte (InTech, 2010)

24. M. Rusu, R. Herda, O.G. Okhotnikov, 1.05- $\mu\text{m}$  mode-locked ytterbium fiber laser stabilized with the pulse train from a 1.54- $\mu\text{m}$  laser diode: errata. *Opt. Express* **12**, 5577–5578 (2004)
25. M. Nakazawa, M. Tokuda, N. Uchida, Continuous-wave laser oscillation with an ultralong optical-fiber resonator. *J. Opt. Soc. Am.* **72**, 1338–1344 (1982)
26. G. Geister, R. Ulrich, Neodymium-fibre laser with integrated-optic mode locker. *Opt. Commun.* **68**, 187–189 (1988)
27. J.D. Kafka, D.W. Hall, T. Baer, Mode-locked erbium-doped fiber laser with soliton pulse shaping. *Opt. Lett.* **14**, 1269–1271 (1989)
28. I.N. Duling, Subpicosecond all-fibre erbium laser. *Electron. Lett.* **27**, 544–545 (1991)
29. K. Tamura, H. Haus, E. Ippen, Self-starting additive pulse mode-locked erbium fibre ring laser. *Electron. Lett.* **28**, 2226–2228 (1992)
30. H. Takara, S. Kawanishi, M. Saruwatari, K. Noguchi, Generation of highly stable 20 GHz transform-limited optical pulses from actively mode-locked Er<sup>3+</sup>-doped fibre lasers with an all-polarisation maintaining ring cavity. *Electron. Lett.* **28**, 2095–2096 (1992)
31. K. Tamura, E. Ippen, H. Haus, L. Nelson, 77-fs pulse generation from a stretched-pulse mode-locked all-fiber ring laser. *Opt. Lett.* **18**, 1080–1082 (1993). cited By 654
32. T.F. Carruthers, I.N. Duling, 10-GHz, 1.3-ps erbium fiber laser employing soliton pulse shortening. *Opt. Lett.* **21**, 1927–1929 (1996)
33. M. Nakazawa, E. Yoshida, A 40-GHz 850-fs regeneratively fm mode-locked polarization-maintaining erbium fiber ring laser. *IEEE Photonics Technol. Lett.* **12**, 1613–1615 (2000)
34. U. Keller, Ultrafast solid-state laser oscillators: a success story for the last 20 years with no end in sight. *Appl. Phys. B* **100**, 15–28 (2010)
35. R. Herda, O.G. Okhotnikov, Dispersion compensation-free fiber laser mode-locked and stabilized by high-contrast saturable absorber mirror. *IEEE J. Quantum Electron.* **40**, 893–899 (2004)
36. M. Rusu, R. Herda, O.G. Okhotnikov, 1.05- $\mu\text{m}$  mode-locked ytterbium fiber laser stabilized with the pulse train from a 1.54- $\mu\text{m}$  laser diode. *Opt. Express* **12**, 5258–5262 (2004)
37. S. Krishnamoorthy, M. Mathew, S. Mayor, A. Prabhakar, Actively mode locked fiber laser for synchronized pulsed depletion in STED, (ThP-T1-P-17) in *6th EPS-QEOD Europhoton Conference, Neuchatel, Switzerland* (2014)
38. S. Krishnamoorthy, D. Jayavel, M. Mathew, S. Mayor, A. Prabhakar, Depletion laser for pulsed sted using wavelength stabilized actively mode locked lasers, in *ICOL, Dehradun, India* (2014)
39. S. Krishnamoorthy, S. Mayor, A. Prabhakar, Synchronization between two fixed cavity mode locked lasers, in *Proceedings of the 5th International Conference on Photonics, Optics and Laser Technology - Volume 1: PHOTOPTICS, INSTICC* (SciTePress, 2017), pp. 273–282
40. H.A. Haus, A theory of forced mode locking. *IEEE J. Quantum Electron.* **11**, 323–330 (1975)
41. C.J. Buczek, R.J. Freiberg, M. Skolnick, Laser injection locking. *Proc. IEEE* **61**, 1411–1431 (1973)
42. D.J. Kuizenga, A. Siegman, FM and AM mode locking of the homogeneous laser-Part I: theory. *IEEE J. Quantum Electron.* **6**, 694–708 (1970)
43. F.X. Kärtner, D. Kopf, U. Keller, Solitary-pulse stabilization and shortening in actively mode-locked lasers. *J. Opt. Soc. Am. B* **12**, 486–496 (1995)
44. L. Nelson, D. Jones, K. Tamura, H. Haus, E. Ippen, Ultrashort-pulse fiber ring lasers. *Appl. Phys. B* **65**, 277–294 (1997)
45. J. Kim, Y. Song, Ultralow-noise mode-locked fiber lasers and frequency combs: principles, status, and applications. *Adv. Opt. Photonics* **8**, 465–540 (2016)
46. A. Takada, H. Miyazawa, 30 GHz picosecond pulse generation from actively mode-locked erbium-doped fibre laser. *Electron. Lett.* **26**, 216–217 (1990)
47. S. Thiruthakkathevan, Scheme for coherent state quantum key distribution. Master's thesis, Indian Institute of Technology Madras, India (2011)
48. B. Razavi, A study of injection pulling and locking in oscillators, in *Proceedings of IEEE Custom Integrated Circuits Conference* (2004), pp. 305–312
49. R. Adler, A study of locking phenomena in oscillators. *Proc. IRE* **34**, 351–357 (1946)

50. K. Kurokawa, Injection locking of microwave solid-state oscillators. *Proc. IEEE* **61**, 1386–1410 (1973)
51. S.H. Strogatz, *Nonlinear Dynamics and Chaos: With Applications to Physics, Biology, Chemistry, and Engineering*. (Westview, Boulder, 2014)
52. A. Siegman, *Lasers* (University Science Books, Sausalito, 1986)
53. S. Krishnamoorthy, A. Prabhakar, Mode unlocking characteristics of an RF detuned actively mode-locked fiber ring laser. *Opt. Comm.* **431**, 39–44 (2019)
54. C. Xu, F. Wise, Recent advances in fibre lasers for nonlinear microscopy. *Nat. Photonics* **7**, 875–882 (2013)
55. F. El-Diasty, Coherent anti-Stokes Raman scattering: spectroscopy and microscopy. *Vib. Spectrosc.* **55**, 1–37 (2011)
56. A. Jonáš, D. McGloin, A. Kiraz, Droplet lasers. *Opt. Photonics News* **26**, 36–43 (2015)